Magnetic Resonance in Medicine 63:1529–1536 (2010)

In Vivo Assessment of Wall Shear Stress in the Atherosclerotic Aorta Using Flow-Sensitive 4D MRI

Andreas Harloff,[1] Andrea Nußbaumer,[1] Simon Bauer,[2] Aurélien F. Stalder,[2] Alex Frydrychowicz,[2] Cornelius Weiller,[1] Jürgen Hennig,[2] and Michael Markl[2]*

Our purpose was to correlate atherogenic low wall shear stress (WSS) and high oscillatory shear index (OSI) with the localization of aortic plaques. Flow-sensitive four-dimensional MRI was used to acquire three-dimensional blood flow in the aorta of 62 patients with proven aortic atherosclerosis and 31 healthy volunteers. Multiplanar data analysis of WSS magnitude and OSI in 12 wall segments was performed in analysis planes distributed along the aorta. Disturbed WSS and OSI were defined as areas exposed to low WSS magnitude and high OSI beyond individual 15% thresholds. Planewise analysis revealed a good correlation ($r = 0.85$) of individual low WSS magnitude but not of high OSI with plaque distribution. Although plaques occurred only rarely in the ascending aorta, the incidence of low WSS magnitude and high OSI was similar to findings in other aortic segments where plaques occurred more frequently. Case-by-case comparisons of plaque location and critical wall parameters revealed a shift of atherogenic WSS magnitude (78% of all cases) and OSI (91%) to wall segments adjacent to the atheroma. Our results indicate that the predictive value of WSS for plaque existence depends on the aortic segment and that locations of critical wall parameters move to neighboring segments of regions affected by atherosclerosis. Magn Reson Med 63:1529–1536, 2010.

Key words: aorta; flow; wall shear stress; MRI; plaque; atherosclerosis

Complex plaques of the aortic arch with thickness $\geq$4 mm or containing thrombi are considered high-risk sources of brain ischemia (1). Cardiovascular risk factors impact on the entire arterial wall and therefore do not explain the focal nature of atherosclerosis preferentially affecting the outer edges of vessel bifurcations and the inner curvature of coronary arteries or the aortic arch (2–4). The close correlation of low and oscillatory wall shear stress (WSS) with local atherosclerotic wall thickening has been shown for the carotid artery bifurcation (5) and in animal models of the aorta and coronary arteries (3,4,6). In human studies, two-dimensional (2D) phase-contrast MRI was applied to analyze WSS in the descending aorta of 10 hypercholesteremic men, and low WSS was able to predict plaque development in single 2D slices in the descending aorta (7). However, the relationship between segmental plaque distribution and WSS in the entire aorta has never been characterized in humans. The accuracy of absolute and oscillatory WSS measurements using three-directional velocity-encoding MRI was recently demonstrated in the aorta of 19 healthy volunteers (8). In contrast to previously described 2D methods (7), flow-sensitive four-dimensional (4D) MRI allows for a full three-dimensional (3D) coverage of the aorta, including regions of highest interest in patients with focal atherosclerotic lesions, i.e., the aortic arch and the outlet of the supra-aortic great arteries (9–15).

We present the first in vivo study investigating the distribution of vector WSS and OSI on eight analysis planes distributed along the thoracic aorta in a large group of patients with proven aortic atherosclerosis. To evaluate the correspondence of WSS and atherosclerosis, the segmental distributions of complex plaques and critical wall parameters were compared. Moreover, to analyze the proximity of WSS and aortic plaques, the individual distance between maximum plaque thickness and regions affected by critical wall parameters was analyzed on a case-by-case basis.

It was our aim to verify if complex aortic plaques were predominantly located in areas with reduced shear stress or increased oscillatory shear index (OSI), or both.

MATERIALS AND METHODS

Study Cohort

Sixty-three nonconsecutive acute stroke patients (mean age = 59.8 ± 13.1 years; 26 females) with acute retinal or cerebral ischemia were prospectively included (see Table 1 for patient demographics). The study cohort, as well as inclusion and exclusion criteria, was previously described in detail (16). Patients were compared with 31 healthy volunteers (mean age = 23.7 years; eight females) from a previous study (17). The study was approved by the local ethics committee and written informed consent was obtained from all participants. Due to insufficient quality of the flow-sensitive 4D MRI data (enhanced noise and susceptibility artifacts in the ascending aorta due to sternal clips) for the analysis of WSS, one patient had to be excluded from analysis. Thus, 62 patients were finally included in the present study.

MRI Experiments

All experiments were conducted on a 3-T MRI system (Trio; Siemens, Erlangen, Germany), using a standard 12-channel torso coil.

[1]Department of Neurology, University Hospital Freiburg, Freiburg, Germany.
[2]Department of Radiology, Medical Physics, University Hospital Freiburg, Freiburg, Germany.

Grant sponsor: Deutsche Forschungsgemeinschaft; Grant number: MA 2383/4-1; Grant sponsor: Bundesministerium für Bildung und Forschung; Grant number: 01EV0706.

*Correspondence to: Michael Markl, Ph.D., University Hospital Freiburg, Department of Radiology, Medical Physics, Breisacher Strasse 60a, 79106 Freiburg, Germany. E-mail: michael.markl@uniklinik-freiburg.de

Received 25 June 2009; revised 5 January 2010; accepted 6 January 2010.
DOI 10.1002/mrm.22383
Published online in Wiley InterScience (www.interscience.wiley.com).

Table 1
Baseline Characteristics of the Study Population

Characteristic, no. (%)	Value, $N = 62$
Hypertension	47 (75.8)
Diabetes	12 (19.4)
Hyperlipidemia	23 (37.1)
Smoking	24 (38.7)
Coronary artery disease	5 (8.1)
Peripheral artery disease	4 (6.5)
History of stroke/transient ischemic attack	12 (19.4)

All patients were screened for aortic plaques, using a bright-blood T_1-weighted radiofrequency-spoiled and fat-saturated 3D gradient echo sequence with an isotropic resolution of ~1 mm^3. To minimize wall motion and breathing artifacts, data were acquired during a short diastolic window (158 ms) combined with respiratory navigator gating. Imaging parameters were as follows: voxel size = 0.8 × 1.1 × 1.1 mm^3; field of view = 350 × 252mm^2; echo time/pulse repetition time = 1.7/5.1 ms; flip angle = 20°. Full axial 3D coverage of the upper thoracic aorta permitted the reliable detection of aortic plaques >4 mm in the ascending aorta, arch, and proximal descending aorta, as described previously (18).

For the individual evaluation of 3D hemodynamics, time-resolved flow-sensitive 4D MRI was employed. Respiration and wall-motion artifacts were minimized by prospective Electrocardiography (ECG) gating and respiratory control using navigator gating of the lung-liver interface (19). Imaging parameters were venc = 150 cm/sec, spatial resolution = 2.1 × 3.2 × 3.0–3.5 mm^3 in a sagittal-oblique 3D volume, with rectangular field of view = 400 × 300 mm^2, flip angle = 15°, echo time/pulse repetition time = 3.5/6.1 ms, temporal resolution = 48.8 ms, slab thickness = 66–77 mm, scan time = 12–20 min, depending on heart rate and navigator efficiency. Data processing included noise filtering, correction for eddy currents, and velocity aliasing as described previously (20).

Data Analysis

A 3D phase-contrast MR angiography was calculated from the 4D MR data, using a home-built analysis tool (MatLab; The MathWorks, Natick, MA, USA) (19,21). Next, commercially available software (EnSight v. 8.2, CEI, Apex, NC, USA) was used to depict the 3D aortic geometry for blood flow visualization and to position eight analysis planes at defined anatomic landmarks normal to the aorta (Fig. 1). Planes were then imported into an in-house analysis tool programmed in MatLab (The MathWorks). Vectorial WSS was directly derived from the flow-sensitive 4D MRI data, using first-order derivatives of measured velocities, which were mapped directly onto the segmented lumen contours, using cubic B-spline interpolation as described previously (8). After segmentation of all measured time frames, absolute time-averaged shear stress (WSS_{mag}) and OSI reflecting the degree of WSS_{mag} inversion over the cardiac cycle were extracted for 12 segments along the vessel circumference. The placement of the analysis plane and definition of the 12 segments for each plane are illustrated in Fig. 1.

Multiplaner reformatting of the bright-blood 3D T_1 gradient echo data (J-Vision; Tiani Medgraph AG, Innsbruck, Austria) was used to detect plaques in the upper thoracic aorta by visual inspection of the images by an experienced observer. For high-risk plaques ≥4 mm, image planes normal to the aorta at the site of the maximum thickness of the detected complex plaques were generated. These 2D imaging planes were imported into the flow visualization software and spatially registered with the flow-sensitive 4D MRI data, as illustrated in Fig. 1. The same 12-segment model used for WSS analysis was also employed to define segments affected by severe atherosclerosis (plaque thickness ≥4 mm occupied at least 50% of the segment area).

Comparison of vessel wall parameters between different patient groups was based on mean WSS_{mag} and OSI for each analysis plane (averaged over segments and time). Patients were divided in groups with severe (plaques ≥4 mm thick or containing mobile thrombi; $n = 34$) or mild atherosclerosis (plaques <4 mm; $n = 28$). Results were compared to identically derived findings in 31 younger healthy volunteers from a previously conducted and reported study (17).

While a number of studies have shown that low WSS and high OSI promote the development of atherosclerotic lesions, no clear quantitative link between altered wall parameters and plaque development is known (2,3). Similar to an approach by Lee et al. (22) and Stone et al. (23), we defined critical atherogenic wall parameters to be present if segments were exposed to WSS_{mag} below (or OSI above) an individual threshold. For the identification of areas at risk for plaque development, i.e., regions affected by critical wall parameters, the segments representing the individual lower 15% of WSS_{mag} and upper 15% of OSI were determined for each patient and volunteer.

Bull's-eye plots were used for a groupwise comparison of the cumulative segmental distributions of critical wall parameters between patients with severe and mild atherosclerosis and the younger volunteers.

For the 34 patients with complex plaques, regional critical WSS_{mag} and OSI were additionally compared to the distribution of the atherosclerotic lesions. For comparison of wall parameters and plaque location, all identified segments were mapped onto the corresponding segment of the nearest WSS analysis plane. Plaques halfway between two analysis planes were considered for both neighboring slices. As a result, a segmental distribution of aortic plaques ≥4 mm was obtained for 34 patients.

Data for this patient group were further evaluated based on the assumption that the distance between critical wall parameters and plaque constitutes potentially important information regarding plaque progression. The individual distance between maximum plaque thickness and the nearest segment affected by critical wall parameters was determined on a case-by-case basis.

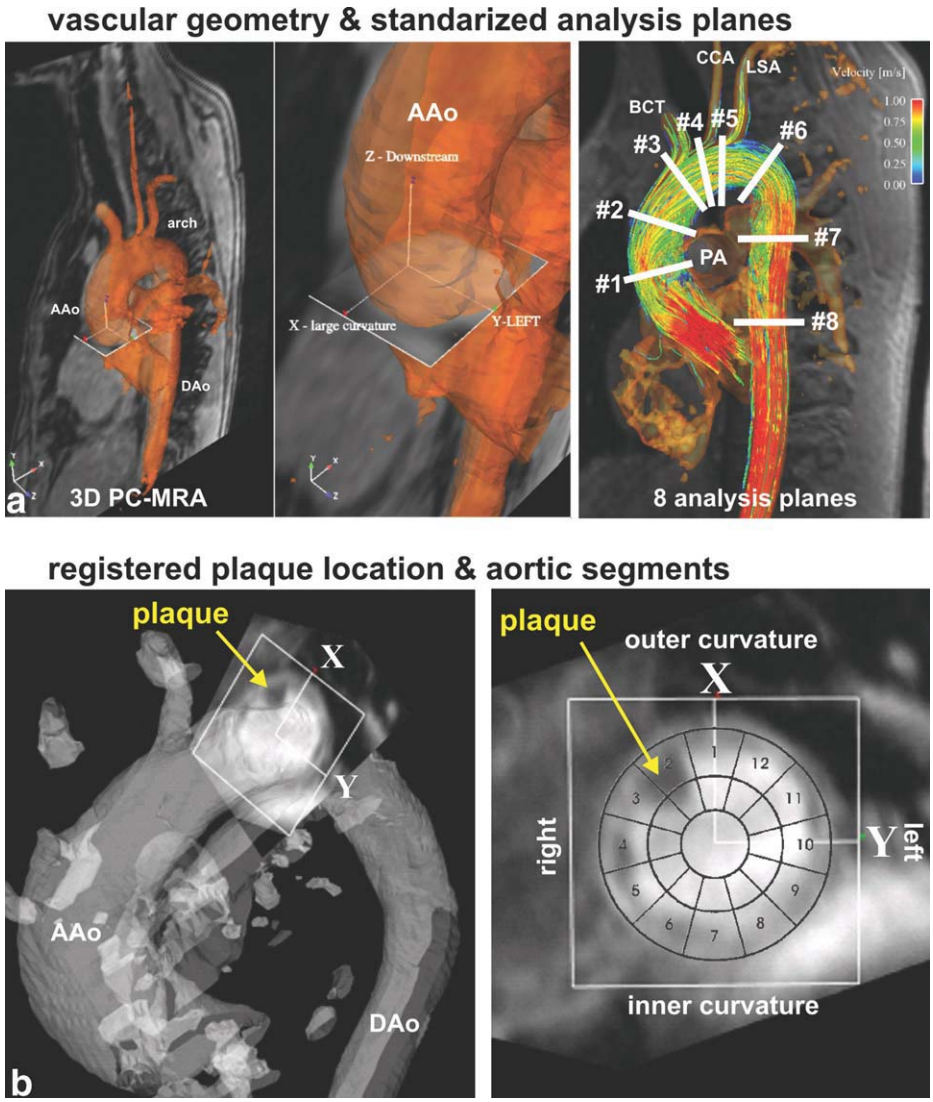

FIG. 1. **a**: Consistent analysis plane orientation and locations for WSS quantification based on the 3D phase-contrast MR angiography geometry. The x-axis was always directed to the outer curvature of the aorta, the y-axis perpendicularly to left aortic wall, and the z-axis pointed downstream. Plane #1 is located in the ascending aorta at the level of the pulmonary artery (PA), plane #3 immediately proximal to the outlet of the brachiocephalic trunk (BCT), and plane #2 in between these planes. Plane #4 is positioned between the outlet of the BCT and the left common carotid artery (CCA), plane #5 between the outlet of the CCA and the left subclavian artery (LSA). Plane #6 lies in the descending aorta (DAo) in the center of the distal aortic arch, #7 at the beginning of the straight segment of the DAo and plane #8 in the distal DAo at the level of the aortic valve. **b**: Definition of aortic segments affected by plaque thickness $\geq$4 mm by image fusion of the detected plaque (large thrombus of the proximal descending aorta, yellow arrow) and the flow-sensitive 4D MRI data. Analysis plane and plaque plane orientation were carefully matched using x and y orientation as precise landmarks. In this case, segments 2 and 3 were affected by plaque thickness $\geq$4 mm. AAo = ascending aorta.

Statistical Analysis

Correlation between the number of segments affected by critical wall parameters and plaque distribution was evaluated on a plane-by-plane basis, using linear regression analysis. The overall quality of the regression was assessed using Pearson's correlation coefficient. Correlations were considered significant for $P < 0.05$.

RESULTS

The total scan time for plaque detection and flow-sensitive 4D MRI in the patients was 56.6 ± 14.8 min. Based on T_1 3D gradient echo imaging, severe atherosclerosis with at least one plaque $\geq$4 mm was found in 34 patients (maximum plaque thickness = 4.9 mm ± 0.8 mm). The atherosclerosis in the remaining 28 patients was classified as mild (maximum plaque thickness = 2.6 mm ± 0.9 mm).

Mean Slice-by-Slice and Global WSS

In patients, mean WSS_{mag} and mean OSI systematically decreased from the ascending to the descending aorta. In contrast, mean WSS_{mag} increased in the descending aorta in younger healthy volunteers, while OSI remained relatively stable for all eight analysis planes (Fig. 2). No

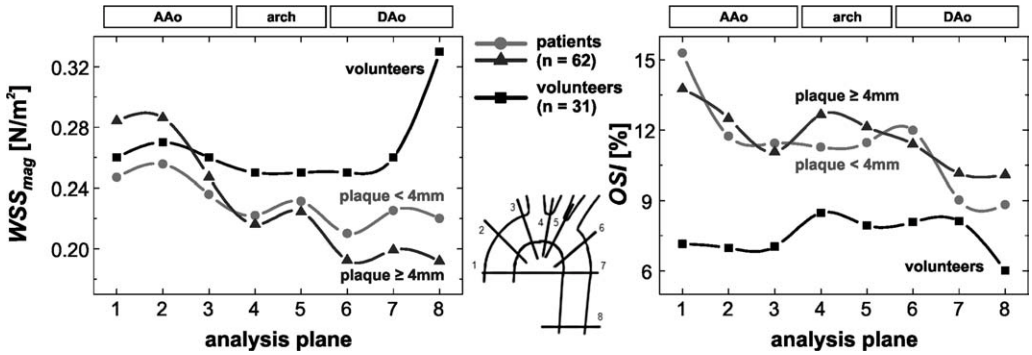

FIG. 2. Distribution of WSS_{mag} (left) and OSI (right) over all eight analysis planes within the thoracic aorta, as indicated by the scheme in the center. The graphs show the comparison of wall-thickness-dependent differences between healthy volunteers and patients.

difference of WSS parameters was found for patients with plaques <4 or ≥4 mm thickness.

Segmental Plaque and WSS Distribution

The distribution of plaque promoting low WSS_{mag} and high OSI for seven analysis planes is shown in Fig. 3 for the 34 patients with complex plaques of the aorta. Critical parameters of WSS_{mag} (lowest 15%) were found in the proximal descending aorta (plane 6) in most of the patients. Interestingly, this was exactly the region with the highest number of segments with a plaque thickness ≥4 mm. Plaque location with respect to analysis planes correlated well ($r = 0.85$; $P < 0.02$) with an increase of the frequency of individual low WSS_{mag}. However, correlation with individual OSI was poor.

Figures 4 and 5 summarize the results of the segmental wall parameter analysis compared to the distribution of detected complex plaques. In Fig. 4, the cumulative distributions of critical wall parameters for both patient groups and the younger volunteers are shown as bull's-eye plots for WSS_{mag} (top row) and OSI (lower row). The grayscale reflects the number of subjects for whom the respective segment was exposed to atherogenic 15% lowest WSS_{mag} and 15% highest OSI.

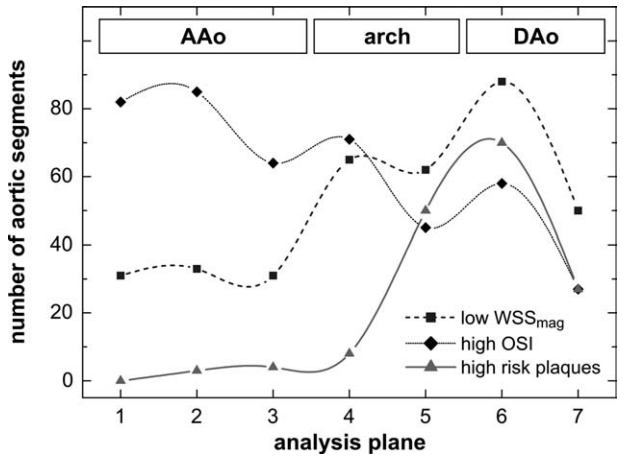

FIG. 3. Distribution of WSS (WSS_{mag}), OSI, and aortic segments affected by complex aortic plaques as a function of analysis plane location. For all analysis planes, the number of segments exposed to low WSS_{mag} correlated well with occurrence of plaques ($r = 0.85$; $P < 0.02$), while no correlation was observed for the distribution of high OSI. As indicated in Fig. 1, analysis planes 1–3 represent the ascending aorta (AAo); planes 4 and 5, the aortic arch; and planes 6 and 7, the proximal descending aorta (DAo).

Segmental high OSI was very pronounced in the left and inner wall of the ascending aorta and of the proximal descending aorta. These areas corresponded well to regions of low WSS_{mag}.

Overall, 34 patients had 53 complex aortic plaques detected by MRI, which could be mapped onto a total of 162 aortic segments in analysis planes 1–7 (Fig. 4, right column). Complex plaques were only found in seven segments (4.3%) of the ascending aorta, 58 segments (35.8%) of the arch, and in 97 segments (59.9%) of the proximal descending aorta. The highest incidence of complex plaques was around plane 6 in the proximal descending aorta. Low WSS_{mag} was found in similar regions affected by complex plaques in the distal aortic arch and the proximal descending aorta. However, for all analysis planes no clear correlation (cc < 0.3) between the segments affected by plaque and low WSS_{mag} was found. Noticeably, there was a high incidence of individual minimum WSS_{mag} and maximum OSI in the ascending aorta both in the 31 healthy volunteers and the 62 patients. However, hemodynamics did not correlate with a high incidence of complex plaques at the same location.

The case-by-case comparison of the location of the maximum thickness of complex plaques relative to the nearest segment affected by critical wall is summarized in Fig. 5. In most cases (73% for WSS; 70% for OSI), at least one segment affected by atherogenic wall parameters (highest/lowest 15% OSI/WSS) was found in the analysis plane closest to the complex plaque (Fig. 5a, distance = 0). In other cases, no clear trend toward an upstream or downstream relocation of the critical wall parameters was observed. Noticeably, as shown in Fig. 5b, in the majority of cases (78% for WSS; 91% for OSI) critical wall parameters for both WSS_{mag} and OSI were shifted to wall segments adjacent to the atheroma. The average difference in location between maximum plaque thickness (mean shift WSS = 3.0 ± 3.2 segments, median = two segments; mean shift OSI = 3.4 ± 2.7 segments, median = three segments) was significantly (t test, $P < 0.001$) different from the hypothesis that the shift does equal 0.

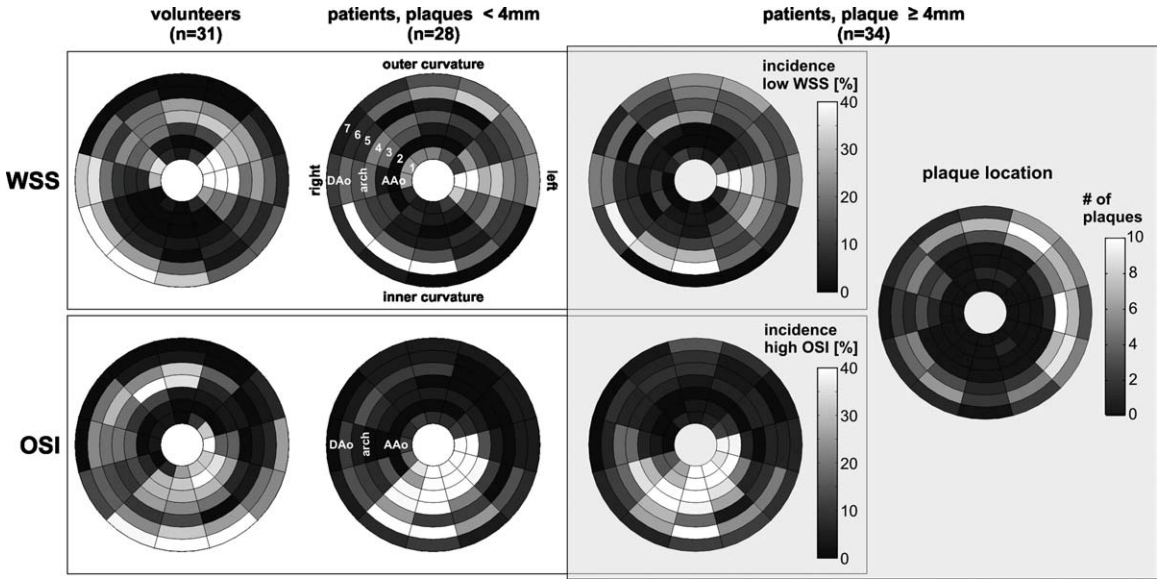

FIG. 4. Segmental occurrence of the individual upper 15% of OSI (lower row) and lower 15% of WSS_{mag} (upper row) in 31 young volunteers and 62 patients. The numbers in each segment represent the number of subjects (incidence in percentage relative to the group size) who had atherogenic low WSS_{mag} or high OSI in the respective aortic region. For 34 patients with complex aortic plaques, the segmental distribution of critical wall parameters is compared with the number of aortic segments (plaque location) affected by a plaque thickness $\geq$4 mm in this group. A moderate correspondence of low WSS_{mag} with plaque location can be appreciated in planes 5–7. However, this was not true for the ascending aorta. High OSI was not correlated with plaque location in this subgroup. Generally, the location of critical wall parameters (low WSS, high OSI) was relocated to aortic areas adjacent to the regions affected by plaques.

DISCUSSION

In the present study, we were able to analyze wall parameters in the entire aortic arch of patients with mild or severe atherosclerosis. Compared to alternative 2D techniques or echocardiography, flow-sensitive 4D MRI permits the spatially nonrestricted evaluation of segmental wall parameters of interest. In addition, data on the distribution of complex plaques showed the direct interrelation with the distribution of WSS parameters within the aorta. Using this approach, it is possible to verify the hypothesis that critical WSS parameters can be found with a higher probability at or near locations that exhibit atherosclerosis.

WSS Distribution

Low WSS_{mag} and high OSI are considered to favor the development and progression of atherosclerosis (2). In our cohort of stroke patients, OSI was not directly correlated with the localization of complex plaques. However, the highest incidence of low WSS_{mag} was observed at the left anterior wall and the inner curvature of the proximal descending aorta and was consistent with the fact that the maximum frequency of wall segments affected by complex plaques was detected at the same site. These findings are in line with previous echocardiographic studies describing that the frequency of complex aortic plaques increases from the ascending to the descending

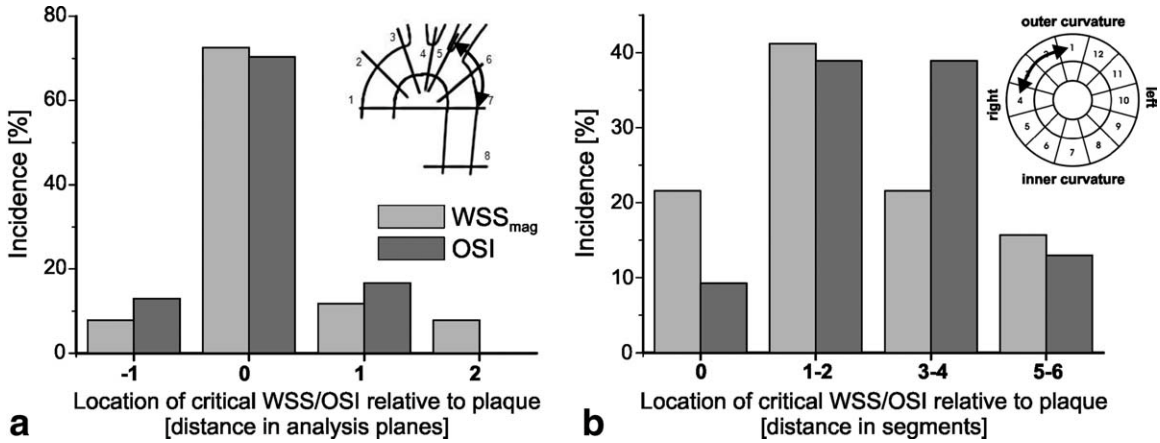

FIG. 5. Case-by-case comparison of the location of the maximum thickness of complex plaques and critical wall parameters with respect to the affected segments (**b**) and analysis plane (**a**).

aorta (1). Thus, it could underline the hypothesis that WSS is a key factor for the occurrence of regional atherosclerosis. Wentzel et al. (7) demonstrated that shear stress predicted the location of wall thickening in the descending aorta in asymptomatic patients with atherosclerosis. However, correlation was relatively low, the ascending aorta and aortic arch were not examined, and topography of hemodynamics and wall thickening of two different groups were compared. Thus, the local distribution of WSS cannot be compared with our results.

In a recent study in 31 healthy volunteers with a mean age of 24 years, Frydrychowicz et al. (17) reported WSS assessment in the aorta, using an MRI method and data analysis strategy that were identical to the present study. Highest OSI and lowest WSS_{mag} moved counterclockwise from the left inner wall of the ascending aorta to the left outer wall of the arch, finally reaching the right inner curvature of the proximal descending aorta. Wall thickness was not measured as part of the protocol, but the distribution of aortic blood flow was in concordance with the description by Kilner et al. (24). Comparable to our patients, the frequency of individual lowest WSS_{mag} and highest OSI was similar in the ascending and descending aorta. However, both in the present study patients and in large cohorts of stroke patients (1), plaques only rarely occur in the ascending aorta. Findings in the proximal aorta are thus conflicting with the hypothesis that critical WSS predicts atherosclerosis.

One explanation could be the fact that we investigated patients with very advanced stages of atherosclerosis, i.e., complex plaques, while most previous studies (2) focused on early atherosclerotic lesions. Furthermore, the ascending aorta is of relatively large diameter compared to the other aortic segments and experiences high and pulsatile blood flow velocities as blood is ejected out of the left ventricular chamber. Compensation for the high pulsatility the ascending aorta serves as a windkessel based on a high number of elastic fibers. The distal arch, however, is a muscular artery type. We thus speculate that, in contrast to current belief (2,3), additional factors such as local wall architecture, intraluminal pressure gradients, and compliance are necessary cofactors to promote local atherosclerosis in the aorta.

Segmental WSS and Plaque Location

The cumulative distributions of critical wall parameters and plaque location (Fig. 4) showed that critical WSS_{mag} and OSI were lowest in the lower half of the descending aorta at the inner curvature in volunteers and patients with both mild and advanced atherosclerosis. In contrast, most plaque segments in this region were found at the left half, which is a 90° counterclockwise rotation. These findings were conformed by systematic case-by-case analysis of the distance between maximum plaque thickness and the nearest segment affected by critical wall parameters. Our data suggest that, during the progression of atherosclerosis, critical wall parameters relocate to neighboring segments of the region most affected by the disease.

Similarly, Cheng et al. (3) demonstrated in an animal model that lowest WSS and highest OSI were not detected at the maximum of the stenosis but proximal and distal to the vessel narrowing, which indicated sites with plaque expansion over time (3). Accordingly, areas with critical aortic WSS identified in our patients could indicate regions at the borders of the existing plaques that are at risk of further plaque progression. The identification of critical WSS in patients with aortic plaques may thus be useful to predict future growth of the atheroma. Future studies are warranted to correlate plaque progression and changes in wall parameter distribution

Limitations

The limited spatial resolution of ~3 mm^3 and temporal resolution of currently ~50 ms of the flow-sensitive 4D MRI data could be responsible for inaccuracies in WSS calculations. An option to improve the accuracy of WSS and OSI estimation may be provided by image-based modeling, using computational fluid dynamics (CFD). A number of applications of CFD for the evaluation of human flow characteristics based on numerical flow simulation in conjunction with realistic vascular geometries and in-flow boundary conditions have been presented (25–28). Wall shear rates have also been derived from CFD results and illustrate the potential of these methods to evaluate wall parameters in 4D (29,30).

It should be noted that CFD calculations in the aorta with its high elasticity and changing stiffness from the ascending to the descending aorta are particularly difficult. The definition of patient-specific vessel wall compliance and vessel motion is challenging, and the direct measurement of flow and WSS using flow-sensitive MRI might be advantageous in these cases.

Direct comparisons of CFD-derived WSS to MR-derived WSS in previous CFD studies thus mostly focused on models of the carotid artery or in vivo data of intracranial aneurysms (31–33). These studies found that WSS assessment based on MRI was feasible but typically underestimated WSS due to limited resolution and spatiotemporal averaging. Therefore, relative values, i.e., individually low WSS_{mag} and high OSI, were used for the analysis of the segmental WSS and OSI distribution since absolute values of WSS were assumed to be significantly underestimated due to the limited resolution in MRI (8). This approach and the current imaging and data analysis techniques proved to be robust and was consistent in healthy volunteers, as shown previously (17).

In this study, full 3D coverage of the aorta instead of multiple 2D scans was chosen for data acquisition, although data evaluation was retrospectively performed on eight analysis planes. Due to the lack of appropriate segmentation algorithms to reliably extract the vessel boundaries in 3D and over time, a true 3D calculation of WSS and OSI could not be performed. Nevertheless, our multiplanar analysis approach is not restricted to predefined 2D analysis planes and could be extended to retrospectively evaluate wall parameters at any location along the aorta.

A drawback of the presented data analysis strategy is related to the manual positioning of analysis planes within the visualization software. In patients with twisted aortic geometries such as kinking or elongation,

the orientation of the 12 segments may not be perfectly aligned with the inner and outer curvature of the aorta. Thus, we assume that a systematical error of ±1 segment for the in-plane analysis of segmental WSS has to be considered. A direct analysis based on an individual one-by-one comparison of plaque location and WSS was currently not performed. Instead, we compared the distribution of WSS in analysis planes next to the site of complex plaques. Since high-risk plaques were thus not directly located on the WSS planes (up to 2-cm distance), we currently do not know the importance of a direct comparison at the same site.

For the calculation of WSS_{mag}, a Newtonian fluid with a viscosity of 4.5 cP was assumed. However, in reality blood is a non-Newtonian fluid, with dependence on the hematocrit level. Thus, the presented approach analyzing relative values seems to provide a reliable comparison of WSS in patients and volunteers and is independent of viscosity changes.

A further limitation is related to the comparison of global and plane-by-plane WSS_{mag} and OSI between patients and the group of much younger normal volunteers. It remains unclear if the changes in WSS and OSI between volunteers and patients are related to the presences of atherosclerosis or differences in age or a combination of both. Future studies should therefore include an age-matched collective of normal controls without atherosclerotic disease to clearly identify the underlying cause of changes in global wall parameters.

These methodological aspects and the design of the study therefore weaken the conclusions of the paper and give strong rationale for further prospective studies. Nevertheless, the presented data agree with previous predictions as to the behavior of WSS in the ascending aorta and may thus be of interest to future CFD or MR studies of the hemodynamics of the thoracic aorta.

The MRI method and data analysis presented here is currently the only technique providing 3D and three-directional data on blood flow in vivo and allows a direct comparison with plaque morphology. Optimization for future studies should particularly focus on an increase of spatial and temporal resolution using parallel-imaging and view-sharing techniques (34–36). Future longitudinal studies using a true 3D detection of plaque localization and WSS distribution in the aorta would be the most reliable approach to study parameters directly influencing plaque occurrence and progression.

In conclusion, flow-sensitive 4D MRI was successfully used to analyze multiplanar WSS distribution in the thoracic aorta of patients with atherosclerosis. Case-by-case analysis revealed a strong correlation between the analysis plane with critical WSS and plaque positions but limited correlation between critical WSS and plaque angular positions. Our results further suggest that the predictive value of WSS for plaque existence depends on the aortic segment and that critical wall parameters relocate to neighboring segments of the region affected by atherosclerosis. Additional factors such as local wall architecture, intraluminal pressure gradients, and compliance may have to be considered to fully understand the development of atherosclerosis in the thoracic aorta.

REFERENCES

1. Kronzon I, Tunick PA. Aortic atherosclerotic disease and stroke. Circulation 2006;114:63–75.
2. Malek AM, Alper SL, Izumo S. Hemodynamic shear stress and its role in atherosclerosis. JAMA 1999;282:2035–2042.
3. Cheng C, Tempel D, van Haperen R, van der Baan A, Grosveld F, Daemen MJ, Krams R, de Crom R. Atherosclerotic lesion size and vulnerability are determined by patterns of fluid shear stress. Circulation 2006;113:2744–2753.
4. Suo J, Ferrara DE, Sorescu D, Guldberg RE, Taylor WR, Giddens DP. Hemodynamic shear stresses in mouse aortas: implications for atherogenesis. Arterioscler Thromb Vasc Biol 2007;27:346–351.
5. Ku DN, Giddens DP, Zarins CK, Glagov S. Pulsatile flow and atherosclerosis in the human carotid bifurcation: positive correlation between plaque location and low oscillating shear stress. Arteriosclerosis 1985;5:293–302.
6. Chatzizisis YS, Jonas M, Coskun AU, Beigel R, Stone BV, Maynard C, Gerrity RG, Daley W, Rogers C, Edelman ER, Feldman CL, Stone PH. Prediction of the localization of high-risk coronary atherosclerotic plaques on the basis of low endothelial shear stress: an intravascular ultrasound and histopathology natural history study. Circulation 2008;117:993–1002.
7. Wentzel JJ, Corti R, Fayad ZA, Wisdom P, Macaluso F, Winkelman MO, Fuster V, Badimon JJ. Does shear stress modulate both plaque progression and regression in the thoracic aorta? Human study using serial magnetic resonance imaging. J Am Coll Cardiol 2005;45:846–854.
8. Stalder AF, Russe MF, Frydrychowicz A, Bock J, Hennig J, Markl M. Quantitative 2D and 3D phase contrast MRI: optimized analysis of blood flow and vessel wall parameters. Magn Reson Med 2008;60:1218–1231.
9. Bolger AF, Heiberg E, Karlsson M, Wigstrom L, Engvall J, Sigfridsson A, Ebbers T, Kvitting JP, Carlhall CJ, Wranne B. Transit of blood flow through the human left ventricle mapped by cardiovascular magnetic resonance. J Cardiovasc Magn Reson 2007;9:741–747.
10. Kvitting JP, Ebbers T, Wigstrom L, Engvall J, Olin CL, Bolger AF. Flow patterns in the aortic root and the aorta studied with time-resolved, 3-dimensional, phase-contrast magnetic resonance imaging: implications for aortic valve-sparing surgery. J Thorac Cardiovasc Surg 2004;127:1602–1607.
11. Markl M, Chan FP, Alley MT, Wedding KL, Draney MT, Elkins CJ, Parker DW, Wicker R, Taylor CA, Herfkens RJ, Pelc NJ. Time-resolved three-dimensional phase-contrast MRI. J Magn Reson Imaging 2003;17:499–506.
12. Wigstrom L, Ebbers T, Fyrenius A, Karlsson M, Engvall J, Wranne B, Bolger AF. Particle trace visualization of intracardiac flow using time-resolved 3D phase contrast MRI. Magn Reson Med 1999;41:793–799.
13. Bogren HG, Buonocore MH. 4D magnetic resonance velocity mapping of blood flow patterns in the aorta in young vs. elderly normal subjects. J Magn Reson Imaging 1999;10:861–869.
14. Buonocore MH. Visualizing blood flow patterns using streamlines, arrows, and particle paths. Magn Reson Med 1998;40:210–226.
15. Wigstrom L, Sjoqvist L, Wranne B. Temporally resolved 3D phase-contrast imaging. Magn Reson Med 1996;36:800–803.
16. Harloff A, Strecker C, Dudler P, Nussbaumer A, Frydrychowicz A, Olschewski M, Bock J, Stalder AF, Stroh AL, Weiller C, Hennig J, Markl M. Retrograde embolism from the descending aorta: visualization by multidirectional 3D velocity mapping in cryptogenic stroke. Stroke 2009;40:1505–1508.
17. Frydrychowicz A, Stalder AF, Russe MF, Bock J, Harloff A, Berger A, Langer M, Hennig J, Markl M. In-vivo vectorial wall shear stress and shear index in the entire human aorta by flow-sensitive 4D magnetic resonance. J Magn Reson Imaging 2009;30:77–84.
18. Harloff A, Dudler P, Frydrychowicz A, Strecker C, Stroh AL, Geibel A, Weiller C, Hetzel A, Hennig J, Markl M. Reliability of aortic MRI at 3 tesla in patients with acute cryptogenic stroke. J Neurol Neurosurg Psychiatry 2008;79:540–546.
19. Markl M, Harloff A, Bley TA, Zaitsev M, Jung B, Weigang E, Langer M, Hennig J, Frydrychowicz A. Time-resolved 3D MR velocity mapping at 3T: improved navigator-gated assessment of vascular anatomy and blood flow. J Magn Reson Imaging 2007;25:824–831.
20. Bock J, Kreher BW, Hennig J, Markl M. Optimized pre-processing of time-resolved 2D and 3D phase contrast MRI data. In: Proc 15th

Annual Scientific Meeting of the International Society for Magnetic Resonance in Medicine, Berlin, Germany, 2007. p 3138.
21. Bock J, Wieben O, Johnson K, Hennig J, Markl M. Optimal processing to derive static PC-MRA from time-resolved 3D PC-MRI data. In: Proc 16th Annual Scientific Meeting of the International Society for Magnetic Resonance in Medicine, Toronto, Canada, 2008. p 3053.
22. Lee SW, Antiga L, Spence JD, Steinman DA. Geometry of the carotid bifurcation predicts its exposure to disturbed flow. Stroke 2008;39:2341–2347.
23. Stone PH, Coskun AU, Kinlay S, Clark ME, Sonka M, Wahle A, Ilegbusi OJ, Yeghiazarians Y, Popma JJ, Orav J, Kuntz RE, Feldman CL. Effect of endothelial shear stress on the progression of coronary artery disease, vascular remodeling, and in-stent restenosis in humans: in vivo 6-month follow-up study. Circulation 2003;108:438–444.
24. Kilner PJ, Yang GZ, Mohiaddin RH, Firmin DN, Longmore DB. Helical and retrograde secondary flow patterns in the aortic arch studied by three-directional magnetic resonance velocity mapping. Circulation 1993;88:2235–2247.
25. Taylor TW, Yamaguchi T. Flow patterns in three-dimensional left ventricular systolic and diastolic flows determined from computational fluid dynamics. Biorheology 1995;32:61–71.
26. Steinman DA, Milner JS, Norley CJ, Lownie SP, Holdsworth DW. Image- based computational simulation of flow dynamics in a giant intracranial aneurysm. AJNR Am J Neuroradiol 2003;24:559–566.
27. Lee SW, Antiga L, Spence JD, Steinman DA. Geometry of the carotid bifurcation predicts its exposure to disturbed flow. Stroke 2008;39:2341–2347.
28. Boussel L, Rayz V, McCulloch C, et al. Aneurysm growth occurs at region of low wall shear stress: patient-specific correlation of hemodynamics and growth in a longitudinal study. Stroke 2008;39:2997–3002.
29. Wood NB, Weston SJ, Kilner PJ, Gosman AD, Firmin DN. Combined MR imaging and CFD simulation of flow in the human descending aorta. J Magn Reson Imaging 2001;13:699–713.
30. Long Q, Xu XY, Bourne M, Griffith TM. Numerical study of blood flow in an anatomically realistic aorto-iliac bifurcation generated from MRI data. Magn Reson Med 2000;43:565–576.
31. Boussel L, Rayz V, Martin A, Acevedo-Bolton G, Lawton MT, Higashida R, Smith WS, Young WL, Saloner D. Phase-contrast magnetic resonance imaging measurements in intracranial aneurysms in vivo of flow patterns, velocity fields, and wall shear stress: comparison with computational fluid dynamics. Magn Reson Med 2009;61: 409–417.
32. Papathanasopoulou P, Zhao S, Kohler U, Robertson MB, Long Q, Hoskins P, Xu XY, Marshall I. MRI measurement of time-resolved wall shear stress vectors in a carotid bifurcation model, and comparison with CFD predictions. J Magn Reson Imaging 2003;17:153–162.
33. Kohler U, Marshall I, Robertson MB, Long Q, Xu XY, Hoskins PR. MRI measurement of wall shear stress vectors in bifurcation models and comparison with CFD predictions. J Magn Reson Imaging 2001; 14:563–573.
34. Markl M, Hennig J. Phase contrast MRI with improved temporal resolution by view sharing: k-space related velocity mapping properties. Magn Reson Imaging 2001;19:669–676.
35. Griswold MA, Jakob PM, Heidemann RM, Nittka M, Jellus V, Wang J, Kiefer B, Haase A. Generalized autocalibrating partially parallel acquisitions (GRAPPA). Magn Reson Med 2002;47:1202–1210.
36. Pruessmann KP, Weiger M, Scheidegger MB, Boesiger P. SENSE: sensitivity encoding for fast MRI. Magn Reson Med 1999;42:952–962.